Experimental Inert Characterization of an Exhaust System Downstream of a CVC

Experimental Inert Characterization of an Exhaust System Downstream of a CVC

Panagiotis Gallis[1], Daniela Anna Misul[1], Bastien Boust[2], Marc Bellenoue[2], and Simone Salvadori[1]

[1]Department of Energy, Politecnico di Torino
[2]Institut PPRIME, CNRS-ENSMA-Université de Poitiers

1 Introduction

Pressure Gain Combustion (PGC) is a pioneering technology that was first introduced in the dawn of the previous century, but only recent progress in aerospace technology has allowed for its further investigation and development [1, 2]. The difference of a conventional combustor and a PGC engine is based on the combustion mode. On the contrary of the considerable induced pressure losses by the conventional burners, PGC machines are able to increase the stagnation properties of the medium during the exothermic process [3]. This specific characteristic increases the theoretical thermal efficiency of the cycle [4] uncovering multiple advantages of the integration of those engines to a Gas Turbine cycle [5].

PGC engines perform with isochoric deflagration [6] or with detonation combustion mode [7, 8]. A prototype PGC engine utilizing the constant volume combustion, namely CVC, has been developed by Boust *et. al* [9]. The peculiarity of these machines is hidden in the pair of rotary intake and exhaust valves. Air is guided inside the chamber and when both valves are closed liquid iso-octane is injected inside. Afterwards, the spark-plug igniter triggers an isochoric combustion. In the end, exhaust valves open and the burned gas is expanded in atmospheric conditions. The combustion event of the engine was experimentally [10] and numerically [11] analysed. In addition, the exhaust system pulsating flow field was numerically investigated using transient 3D CFD calculations [12, 13].

The goal of this paper is to present the newly manufactured exhaust system of CVC. In particular, the new exhaust design is experimentally investigated under inert conditions. First, the experimental test rig is described and then the results of the experimental campaign are discussed. The new exhaust system is able to accelerate the CVC's pulsating outflow and offers a more uniform vertical velocity profile. These findings are promising for the CVC integration with a High-Pressure Turbine stage.

2 Experimental Test Rig

In Fig. 1a the experimental test rig is depicted. The intake supply line feeds the intake tank (1) with air in low temperature (14 ^{o}C), but high pressure (4 bar). Afterwards, the air is guided inside the intake plenum (2). When the rotary inlet valves are open, the medium enters the combustion chamber (3). It must be underlined that no fuel injection or ignition occurs in this specific experimental campaign. When the exhaust valves open, the air is expanded through the exhaust part to atmospheric conditions. The exhaust part consists of a rectangular duct (4) and the newly designed exhaust system (5). In fact, the newly manufactured exhaust system can be identified in a 3D view of Fig. 1b and in a cross section view of Fig. 1c. The exhaust system consists of a transition duct (i) which has a goal to smoothly accelerate the gas. This duct derived after unsteady CFD optimization techniques [14]. A change area duct (ii) is followed which has as a goal to isometrically change the rectangular outlet area of the transition duct to a circular cross-section area. Finally, the exhaust system ends with the converging-diverging circular nozzle (iii), which has a throat diameter of 20 mm.

In this experimental campaign fast response pressure and Particle Image Velocimetry (PIV) measurements are conducted. For the pressure measurements, a Kistler 4011 recessed sensor is implemented in the CVC chamber's walls (P_{cc}). In addition, a Kistler 4007 recessed sensor is placed upstream of the transition duct (P_1), while a Kistler 4049 flush-mounted sensor is positioned downstream of the transition duct (P_2). The sampling frequency of these sensors is 100 kHz. As it can be identified by Fig. 1b, the exhaust system is equipped with two planar glasses mounted in the top and in the lateral

Correspondence to: daniela.misul@polito.it

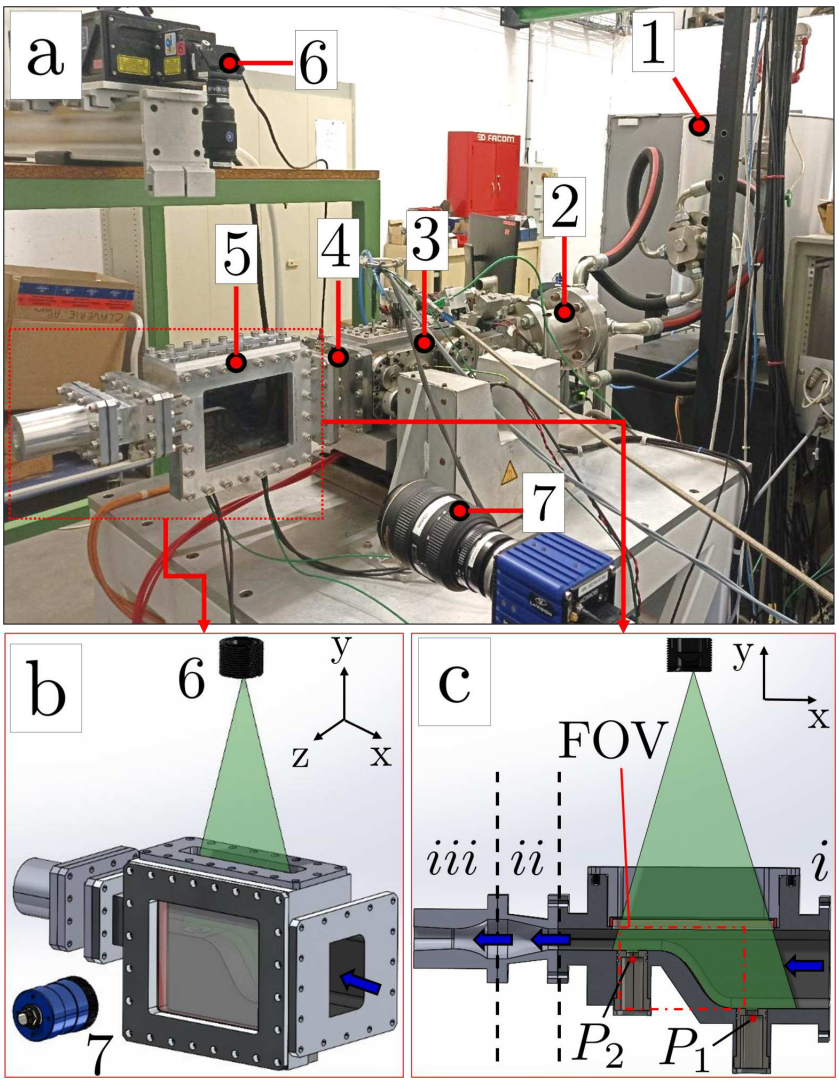

Fig. 1. Experimental Test Rig and Exhaust System.

side of the exhaust system. The top window allows for the penetration of the laser sheet (6), while the lateral window (7) permits visual access inside of transition duct. In fact, the field of view of the camera (FOV) is portrayed in Fig. 1c.

Quantel Evergreen (6) is utilised to create a laser sheet of $2 \cdot 100$ mJ/pulse with a frequency of 25 Hz. The Imager sCMOS camera (7) has a resolution of 2560×2160 pixels with a pixel size of $6.5\mu m \times 6.5\mu m$. The Programmable Timing Unit (PTU X) synchronizes the laser sheet and the opening-closing of camera lens. Seeding of silicon oil droplets occurs upstream in the intake tank (1). An interrogation window of 16×16 pixels with 25 % overlap is used with the help of Davis 10. commercial software to deduce the velocity field in the transition duct domain. It should be stressed that the laser sheet is located in the middle of the transition duct width ($z-$ direction) scanning the pressure sensors P_1 and P_2.

The valves rotation is set to 750 rpm (12.5 Hz). During one rotation, the valves open twice resulting in an effective frequency of 25 Hz. Despite of the absence of combustion, the fast motion of the valves creates a process of filling-emptying of the combustion chamber. Hence, the exhaust system experiences strong inlet pressure fluctuations. The low frequency PIV system has an equal frequency of 25 Hz with the valves. As a result, for each cycle only one PIV event can occur. In fact, the cycle is split into 20 segments with a constant time delay of 2 ms. For the first time delay (10 ms), the machine operates and the acquisition of 200 cycles takes place. The PIV system acquires 200 different flow fields of the same time delay of 10 ms. By averaging 200 instantaneous velocity fields, the average velocity field is obtained. Similarly, the flow field characterisation is obtained for the other 19 time moments. Thus, the PIV system offers the ensemble average velocity field of the transition duct for 20 different moments of the valve's cycle.

3 Results

In Fig. 2, the lift law of intake and exhaust valves is shown with the dashed blue and red curves respectively. For one rotation of the valves ($T_{rot} = 80\ ms$), two periods of pressure fluctuation ($T_p = 40\ ms$) occur as the valves open and close twice. In parallel, the dashed black vertical lines indicate the time moments in which the averaging PIV analysis is performed. It is evident that the PIV acquisition covers 1 full period of pressure fluctuations with 20 different time moments. After the acquisition of the chamber, upstream and downstream of transition duct pressure signals, the Phased-Locked Average (PLA) is performed for one rotational period. The evolutions of these three PLA signals are placed in Fig. 2.

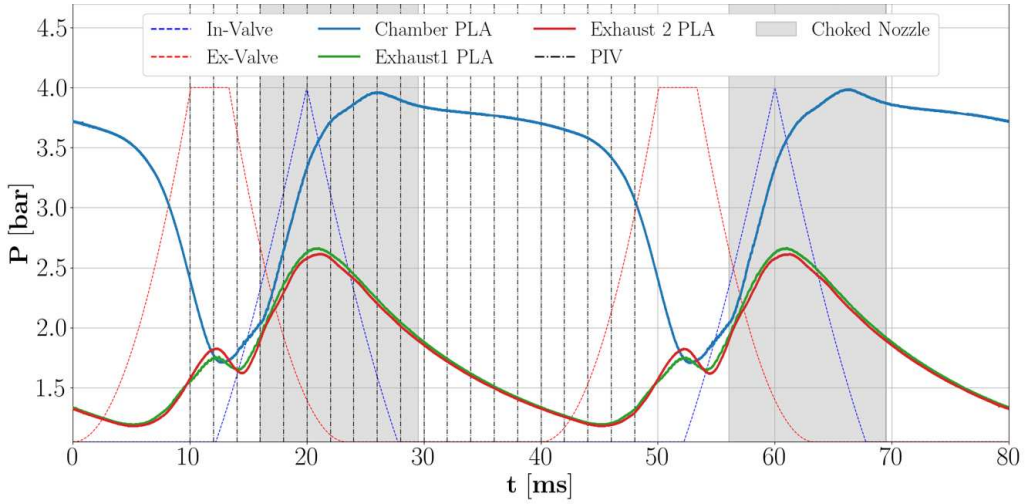

Fig. 2. Operation of CVC and Phase-Locked Average of Chamber, Upstream and Downstream Sensors.

In the start of the cycle ($t = 0\ ms$), the exhaust valves are closed and the chamber is full of air, while the exhaust system expands the last amount of air by the previous cycle. As the exhaust valves open ($t = [0 - 12]\ ms$) and the intake valves are still closed, the chamber's pressure rapidly decreases while a rise of upstream and downstream of transition duct signals is observed. With the opening of the intake valves, the pressure inside of chamber augments again triggering a simultaneous rise of the exhaust sensors signals. In fact, the elevated pressure reported by P_1 can indicate if the exhaust nozzle, which expands the air in atmospheric conditions, is choked or not. The grey shaded area denotes the time window when the pressure ratio with the help of P_1 is below the critical one. The pressure upstream and downstream of the transition duct continues to rise till the moment of the closing of the exhaust valves ($t = 22\ ms$). Later, the exhaust system expands the air with a smooth continuous pressure decay, while the chamber's pressure remains almost constant after the intake valves closing ($t = 28\ ms$). The sequential operation of the system repeats again in the second half of the rotational period ($t = [40 - 80]\ ms$).

In Fig. 3, an example of flow field at 10 ms is displayed. In particular, Fig. 3b presents the velocity field of the transition duct. At 10 ms the exhaust valves are fully open with closed intake valves. The chamber's pressure approaches the exhaust system's sensors pressure denoting the fully expansion of trapped air inside of the chamber. This leads to a huge recirculation zone which can be identified in the inlet of the transition duct. Moreover, a stagnation point of this vortex is identified at its collision with the upper window wall (white zone in $x = -25\ mm,\ y = 75$). On the contrary, the transition duct outlet is characterised by a uniformly accelerated flow.

Fig. 3a depicts the non-dimensional velocity profile along the vertical direction for the inlet and outlet of the transition duct. In fact, the vertical velocity profile is divided by the maximum local velocity module of the inlet and outlet respectively. The vortical structure in the inlet can be detected by the alternation of the sign of the inlet profile at $y_i/dy_i = 0.5$. On the other hand, the outlet velocity profile is very uniform. An interesting statistical quantity is the coefficient of variance (COV) of the velocity profiles. The inlet velocity profile has a COV equal to 9.72, while the outlet only 0.13. For this specific moment, the transition duct manages to homogenize significantly the outflow of the CVC

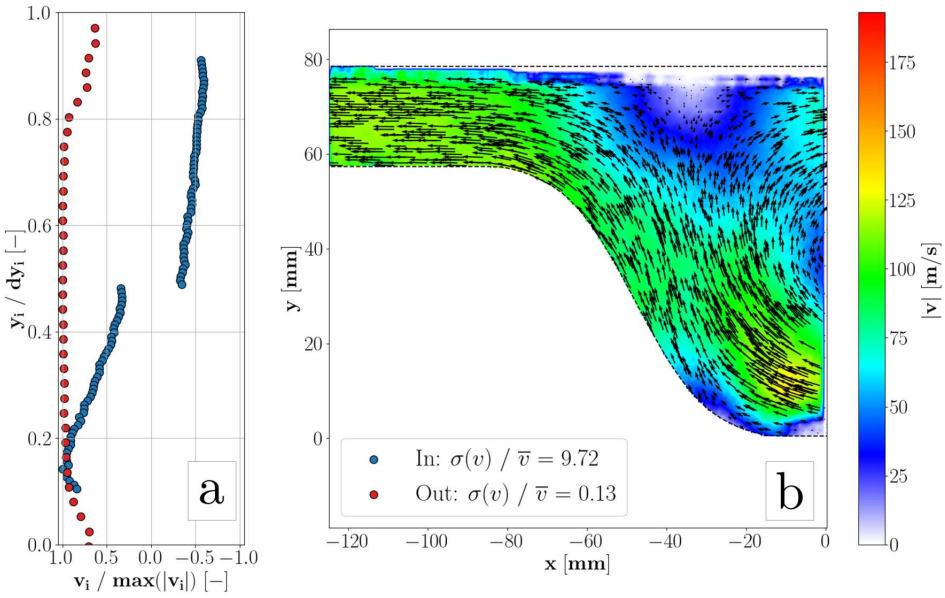

Fig. 3. Average PIV Velocity Flow Field at $t = 10\ ms$.

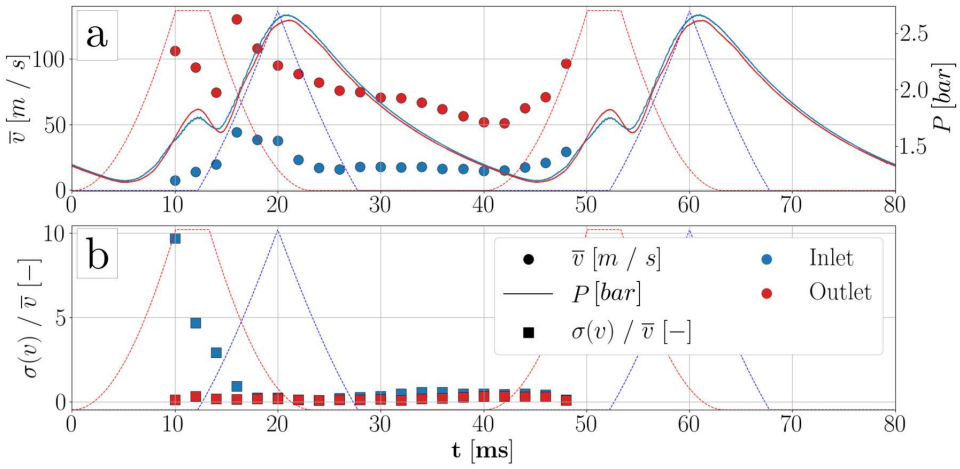

Fig. 4. Evolution of Average Velocity and Coefficient of Variance of Velocity Profile.

in the vertical direction.

The statistical analysis of the 10 ms case is performed for the rest of 19 moments. In Fig. 4a, the left graph abscissa corresponds to the evolution of the local average velocity at inlet and outlet of the transition duct. On the other hand, the right graph abscissa refers to the pressure evolution at the inlet and outlet of the transition duct. Regardless the low inlet velocity, the transition duct manages to keep the outlet velocity always above of 50 m/s, while it achieves a maximum velocity of 130 m/s. In parallel, Fig. 4b offers the evolution of the velocity profile coefficient of variance for the inlet and outlet of the transition duct. The transition duct achieves to provide a flow field with a significant lower coefficient of variance for every time moment. Thus, the newly designed exhaust system offers a more uniform velocity distribution in the vertical direction of the middle section for every moment of the pulsation.

4 Conclusions

The present manuscript describes the inert experimental campaign of the CVC test rig equipped with the new exhaust system. Air in low temperature (14 ^{o}C) and elevated pressure (4 bar) is guided inside of chamber and periodically expanded through the exhaust system to atmospheric conditions. The exhaust system is designed to offer visual inspection of the flow field which is previously seeded with silicon oil particles. In fact, an arrangement of two windows allows for PIV measurements of the oscillating exhaust field. In addition, ports in the CVC and in the transition duct's inlet and outlet monitor the evolution of static pressure.

The transition duct achieves to accelerate the flow field and to uniformize vertically the velocity profile for every time moment. The outlet of duct preserves velocity levels above 50 m/s during a cycle. In particular, the excessive perturbing flow field at the inlet of the transition duct is significantly homogenised at the outlet. The inlet of the exhaust system is highly affected by the opening and closing of exhaust valves, whilst the outlet of duct achieves a COV of vertical velocity profile lower than 0.35 during the cycle. These findings are very promising for turbomachinery applications. The new exhaust system accomplishes to provide a continuous accelerating flow in which vertical distortions are absent. Thus, the combustion benefits of CVC will not be counteracted by imposing spatial non-uniformities to a subsequent turbine. Next step of the activity will be the characterisation of the exhaust system with high-frequency PIV for the active cases.

Acknowledgement

The present activity is performed in the frame of the INSPIRE project (Grant Agreement 956803) funded by the European Commission through a Marie Sklodowska-Curie action. The authors would like to deeply thank Alain Claverie for his support and contribution in the experimental campaign.

References

[1] Piotr Wolański. Detonative propulsion. *Proceedings of the Combustion Institute*, 34(1):125–158, 2013.

[2] Irvin Glassman, Richard A. Yetter, and Nick G. Glumac. Flame phenomena in premixed combustible gases. In *Combustion*, chapter 4, pages 147–254. Academic Press, Waltham, 5 edition, 2015.

[3] G. Ciccarelli and S. Dorofeev. Flame acceleration and transition to detonation in ducts. *Progress in Energy and Combustion Science*, 34(4):499–550, August 2008.

[4] William H. Heiser and David T. Pratt. Thermodynamic cycle analysis of pulse detonation engines. *Journal of Propulsion and Power*, 18(1):68–76, January 2002.

[5] Jorge Sousa, Guillermo Paniagua, and Elena Collado Morata. Thermodynamic analysis of a gas turbine engine with a rotating detonation combustor. *Applied Energy*, 195:247–256, June June 2017.

[6] Panagiotis Stathopoulos, Johann Vinkeloe, and Christian Oliver Paschereit. Thermodynamic evaluation of constant volume combustion for gas turbine power cycles. In *Numerical Set Updings of the 11th International Gas Turbine Congress*, pages 15–20, Tokyo, Japan, 2015.

[7] H Douglas Perkins and Daniel E Paxson. Summary of pressure gain combustion research at nasa. Technical report, NASA / TM-2018-219874, April 2018.

[8] Manabu Hishida, Toshi Fujiwara, and Piotr Wolanski. Fundamentals of rotating detonations. *Shock Waves*, 19(1):1–10, April 2009.

[9] Bastien Boust, Quentin Michalski, and Marc Bellenoue. Experimental investigation of ignition and combustion processes in a constant-volume combustion chamber for air-breathing propulsion. In *52nd AIAA/SAE/ASEE Joint Propulsion Conference*, page 4699, Salt Lake City, UT, July 2016. AIAA.

[10] Bastien Boust, Marc Bellenoue, and Quentin Michalski. Pressure gain and specific impulse measurements in a constant-volume combustor coupled to an exhaust plenum. In *Active Flow and Combustion Control 2021*, pages 3–15, Berlin, Germany, 2022. Springer.

[11] Laure Labarrere, Thierry Poinsot, Antoine Dauptain, Florent Duchaine, Marc Bellenoue, and Bastien Boust. Experimental and numerical study of cyclic variations in a constant volume combustion chamber. *Combustion and Flame*, 172:49–61, October Oct. 2016.

[12] Panagiotis Gallis, Daniela Anna Misul, Simone Salvadori, Marc Bellenoue, and Bastien Boust. Development and validation of a 0-d/1-d model to evaluate pulsating conditions from a constant volume combustor. In *Joint Meeting of International Workshop on Detonation for Propulsion (IWDP) and International Constant Volume and Detonation Combustion Workshop (ICVDCW)*, Berlin, Germany, 15-19 August, 2022.

[13] Panagiotis Gallis, Daniela Anna Misul, Marc Bellenoue, Bastien Boust, and Simone Salvadori. Development of 1d model of constant-volume combustor and numerical analysis of the exhaust nozzle. *Energies*, 17(5):1191, 2024.

[14] Panagiotis Gallis, Daniela Anna Misul, Marc Bellenoue, Bastien Boust, and Simone Salvadori. Numerical analysis and design of new exhaust section downstream of constant volume combustor. In *Turbo Expo: Turbomachinery Technical Conference and Exposition*. American Society of Mechanical Engineers, 2024.